

# Interactions between synoptic, intraseasonal and interannual convective variability over Southern Africa

B. Pohl · N. Fauchereau · Y. Richard ·  
M. Rouault · C. J. C. Reason

Received: 10 June 2008 / Accepted: 16 October 2008 / Published online: 7 November 2008  
© Springer-Verlag 2008

**Abstract** After removing the annual cycle, a principal component analysis is applied to the daily outgoing long-wave radiation anomaly field, used here as a proxy for atmospheric convection. The analysis is carried out over the southern African region (7.5°E–70°E, 10°S–40°S) for austral summer (November through February) for the period 1979–1980 to 2006–2007. The first five principal components (PC) are retained. The first two PCs describe spatial patterns oriented north-west to south-east from tropical southern Africa (SA) to the mid-latitudes. They are interpreted to be different possible locations for synoptic-scale tropical–temperate troughs (TTT), one dominant rainfall-producing synoptic system in the region. The phase relationship between these two PCs describes a tendency for these TTT to propagate eastwards from SA to the Mozambique Channel and southern Madagascar. The next three PCs describe convective fluctuations, respectively, located over the north-west, the south and the centre of SA. Their time series are significantly associated with Madden–Julian oscillation (MJO) activity in the tropics. However, we find that TTT systems are statistically independent of the MJO, i.e. they are equally liable to occur during any phase of the MJO. Three PCs out of five also show a significant association with El Niño southern oscillation, confirming that El Niño years mostly coincide with

suppressed convection at the intraseasonal time-scales, a result consistent with its impact on seasonal averages diagnosed in previous studies.

**Keywords** OLR · Atmospheric convection · Summer rainfall · Southern Africa · Principal component analysis · Tropical–temperate troughs · Madden–Julian oscillation · El Niño southern oscillation

## 1 Introduction

Due to the predominance of rain-fed agriculture in Southern Africa (SA, south of 15°S), large departures in the seasonal rainfall amounts (either drought or floods) can have particularly detrimental effects on the economies and societies of the region (Mason and Jury 1997; Reason and Jagadheesha 2005). For instance, Jury (2002) estimated that over U.S.\$1 billion could be saved annually with reliable long range seasonal forecasts. The distribution of rainfall within the rainy season, i.e. the respective length and intensity of the dry and wet spells and their succession is, however, as fundamental as seasonal amounts for agriculture. Studies of rainfall processes on the subseasonal (i.e. the meso-, synoptic or intraseasonal) scale that affect the region, and their relationships with interannual variability, are therefore needed to refine existing knowledge based mostly on monthly means.

The present work investigates the main modes of convective variability over the SA region during austral summer (November through February, “NDJF”), corresponding to the peak of daily rainfall amounts over most of the area. Todd and Washington (1999), Washington and Todd (1999), and more recently Fauchereau et al. (2008)

---

B. Pohl (✉) · Y. Richard  
Centre de Recherches de Climatologie,  
CNRS/Université de Bourgogne,  
6 boulevard Gabriel, 21000 Dijon, France  
e-mail: benjamin.pohl@u-bourgogne.fr

N. Fauchereau · M. Rouault · C. J. C. Reason  
Department of Oceanography,  
University of Cape Town,  
Cape Town, South Africa

highlighted the predominant role of tropical–temperate interactions in the seasonal rainfall amounts over SA. Todd et al. (2004) estimated for instance that synoptic-scale tropical–temperate troughs (TTT) account for 30% (60%) of the overall rainfall amount over SA during the October–December season (January). These TTT systems basically consist of large-scale bands of clouds, convection and rain, oriented in a North-West to South-East direction over SA and the South-West Indian Ocean (SWIO). TTT typically develop when a tropical perturbation in the lower layers (e.g. an easterly wave) meets a mid-latitude trough in the upper atmosphere (Lyons 1991). They were also shown to be related to the establishment of the South-Indian convergence zone (SICZ, Cook 2000). SA and the SWIO is one of the three known preferred regions in the Southern Hemisphere for the occurrences of such cloud alignments (Streten 1973). Unlike its counterparts, namely the South Atlantic and South Pacific convergence zones (SACZ and SPCZ), the SICZ is, however, mainly restricted to the austral summer.

At longer timescales, Pohl et al. (2007) identified an influence of the Madden–Julian oscillation (MJO, Madden and Julian 1994; Zhang 2005) in the alternation of wet and dry phases over SA during the summer rainy season. The MJO basically consists in a mean eastward propagation of large-scale convective clusters ( $\sim 10,000$  km across) along the equator, from the Indian Ocean to the Maritime Continent of Indonesia, and then to the West Pacific basin. The time taken by the MJO to rejuvenate over the Indian Ocean is typically between 40 and 50 days. Over the SA region, the MJO modifies the direction of the lower-layer moisture fluxes, through an influence on the Mascarene High. Anticyclonic anomalies in the Mascarene High generate easterly flux anomalies in the southern low latitudes and northerly anomalies over tropical Africa, favouring moisture transport from the Indian basin to the SA region and above average rainfall there. On the other hand, cyclonic anomalies in the Mascarene High favour southerly anomalies over tropical Africa and dryness over SA. The large-scale convective clusters associated with the MJO over SA were seen to propagate on average from Angola to South Africa, and then northward towards Tanzania and the Great Lakes (Pohl et al. 2007).

Interannual variability in SA rainfall is strongly influenced by the El Niño southern oscillation (ENSO) (Dyer 1979; Lindesay 1988; Lindesay and Vogel 1990; Reason et al. 2000). El Niño events tend to correspond to severe droughts over SA (Rouault and Richard 2003, 2005), however, this relationship is non-linear (e.g. the strong 1997/1998 event was not associated with widespread dry conditions, see Reason and Jagadheesha 2005) and undergoes interdecadal modulation (Richard et al. 2000, 2001; Reason and Rouault 2002).

The interactions between TTT, MJO and ENSO, their respective influences and their cumulative effects on rainfall variability over SA are not well understood. For example, although it has been established that the MJO affects convection in the SACZ (Carvalho et al. 2004) and the SPCZ (Matthews et al. 1996), it is not known if it modulates the frequency or intensity of TTT systems in the SICZ. The imbrication of the synoptic-scale TTT systems and the MJO pseudo-cycle constitutes thus the first scope of this paper. The potential interactions between ENSO-related convective anomalies and the synoptic (intraseasonal) TTT (MJO) activity and their consequences on rainfall remain also to be established. These potential scale interactions with interannual variability constitute the second scope of this paper.

The study is organized as follows. Section 2 describes the datasets and the methodology while Sect. 3 presents the results of the principal component analysis (PCA) (see Sect. 2 for details). The associated atmospheric dynamics and their consequences for South African rainfall are discussed in Sect. 4. Section 5 investigates the relationships between the retained principal components (PCs) and MJO activity in the Tropics. In Sect. 6, focus is given to the interannual component of the PCs, and especially their association with ENSO. Section 7 describes the scale interactions between the synoptic, intraseasonal and interannual timescales. Finally, Sect. 8 contains the summary and discussion.

## 2 Data and methods

Tropical convection is estimated through the daily version of the outgoing longwave radiation (OLR) dataset (Liebmann and Smith 1996). It is available on a  $2.5^\circ \times 2.5^\circ$  regular grid from 1974, with a 10-month gap in 1978. The study period has been restricted to 1979–1980 to 2006–2007 to match the NCEP-2 reanalysis period.

Daily rainfall amounts over the Republic of South Africa are provided by the rain-gauge records compiled in the Water Research Commission database by Lynch (2003). Seven thousand and six hundred and sixty-five stations (out of 11,000), presenting no missing values, are extracted for the 1979–1980 to 1998–1999 period. These data represent rainfall over South Africa and the neighbouring countries of Lesotho, Swaziland and Southern Namibia at relatively high resolution. The use of such a database makes it possible to relate daily OLR variations to the actual precipitation field.

Atmospheric circulation is examined using the NCEP-DOE AMIP-II (NCEP-2) reanalyses (Kanamitsu et al. 2002). This study makes use of the zonal ( $U$ ,  $\text{m s}^{-1}$ ), meridional ( $V$ ,  $\text{m s}^{-1}$ ) and vertical ( $\omega$ ,  $\text{Pa s}^{-1}$ ) components

of the wind. The 500 hPa level represents the center of mass for the troposphere, thus examination of the 500 hPa omega field allows for an insight into large-scale vertical movements in the whole troposphere.

Monthly Sea surface temperatures (SST) are obtained from the HadISST dataset (Rayner et al. 2003) on a  $1^\circ \times 1^\circ$  regular grid, for the 1950-present period. Only NDJF seasonal means and anomalies are used here.

The ENSO signal is extracted using the multivariate ENSO index (MEI, Wolter and Timlin 1993) provided by the Climate Diagnostic Center (<http://www.cdc.noaa.gov>). This bimonthly index, based on both atmospheric and oceanic fields, is adequate to describe the coupled nature of the ENSO phenomenon.

The MJO signal is extracted through the real-time daily indices developed by Wheeler and Hendon (2004, hereafter referred to as WH04). The indices are the PC time series of the two leading empirical orthogonal functions (EOFs) of combined daily mean tropical (averaged  $15^\circ\text{N}$ – $15^\circ\text{S}$ ) 850- and 200-hPa zonal wind and OLR anomalies. WH04 subtracted the annual cycle and the low-frequency variability associated with ENSO before calculating the EOFs. The indices, denoted real-time multivariate MJO (*RMM*)1 and *RMM*2, were designed to be used in real time and to capture both the northern winter and summer MJO. *RMM*1 and *RMM*2 are approximately in quadrature and describe the average large-scale, eastward-propagating convective and circulation anomalies associated with the MJO. The evolution of the MJO can be concisely visualized in a two-dimensional phase–space diagram, with *RMM*1 and *RMM*2 as the horizontal and vertical Cartesian axes, respectively. A polar coordinate representation can also be used (Matthews 2000) in this phase space, where  $A$  is the amplitude ( $A > 0$ ) defined as:

$$A(t) = \sqrt{RMM1^2(t) + RMM2^2(t)}$$

and  $\alpha$  is the phase angle in radians ( $0 \leq \alpha \leq 2\pi$ ):

$$\alpha(t) = \tan^{-1}\left(\frac{RMM2(t)}{RMM1(t)}\right)$$

In this paper, we both use the polar and Cartesian notation of the MJO. In the second case, *RMM*1( $t$ ) is retained as a single descriptor of the global-scale MJO activity.

The present work is based on a PCA, a methodology enabling to constitute continuous (score) time series, which is particularly adequate to focus on temporal scale interactions and imbrications (for all the timescales comprised between the resolution of the input data and the overall length of the period of analysis). Another method, that we used in Fauchereau et al. (2008), is based on a cluster analysis and is more optimal to discriminate recurrent regimes—which is not the scope here.

The PCA presented in this study makes use of the correlation matrix. It is applied to the daily OLR anomalies after removal of the annual cycle in each OLR grid point. The period analyzed (November to February 1979–1980 to 2006–2007) corresponds to the peak of the rainy season over almost all of SA. The domain over which the PCA is applied is  $7.5^\circ\text{E}$ – $70^\circ\text{E}$ ,  $10^\circ\text{S}$ – $40^\circ\text{S}$ . This domain has been successfully used in several previous studies of SA climate variability, particularly those related to tropical–temperate interactions (e.g. Todd and Washington 1999; Washington and Todd 1999; Todd et al. 2004; Fauchereau et al. 2008). The dimension of the input matrix is thus 338 variables (i.e. grid points: 26 in the longitudinal dimension, 13 in the latitudinal dimension) and 3,360 observations (i.e. days: 120 days for each season, 28 years of records).

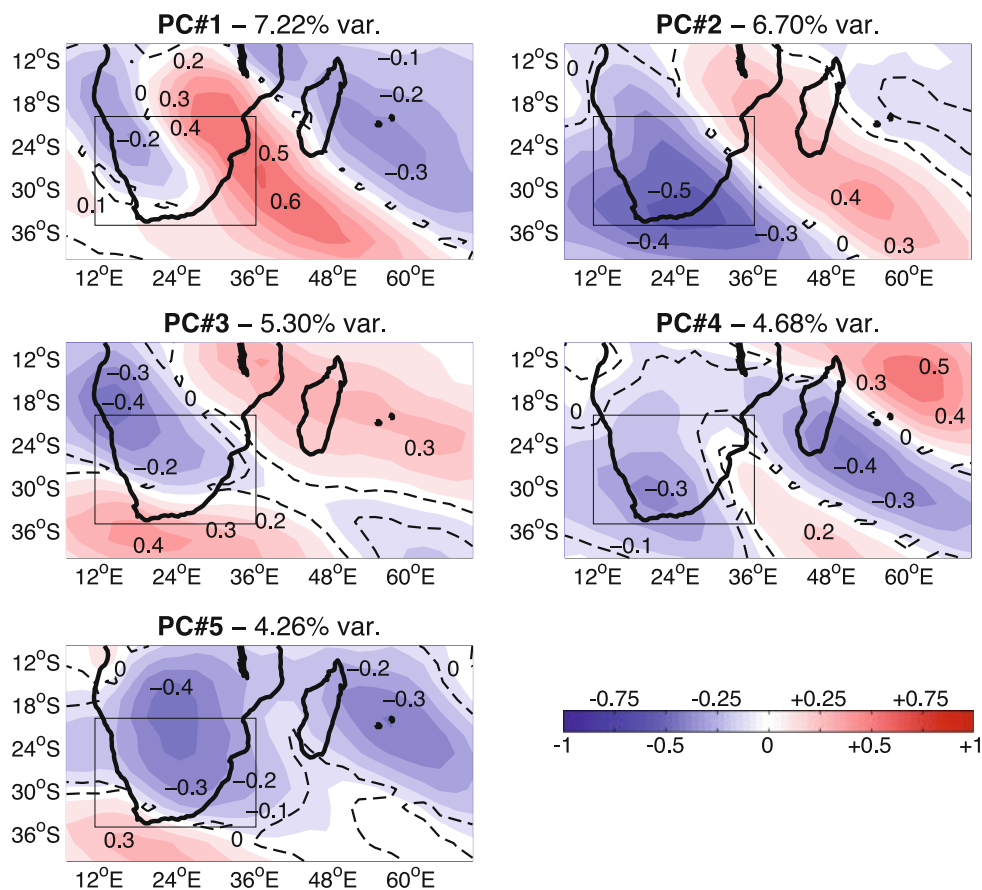
For the remainder of this study, the first five PCs are retained. They explain around 28.2% of the original variance and are significant according to a scree-test. We modified the sign of some PCs, so that the positive phases for each of them corresponds to above-normal rainfall amounts over SA. The results of the PCA are presented in Sect. 3.

### 3 Results of the principal component analysis

Figure 1 presents the spatial patterns (correlation field) associated with the five PCs. The associated time series are not shown here because of the large number of days included in this analysis. In order to document the timescales at which these structures vary, Fig. 2 presents a wavelet analysis (Torrence and Compo 1998) applied to the scores of the five PCs. The methodology used here is the same as in Prokoph and Patterson (2004). For readability, the wavelet scalograms were averaged over the 28 years of records. As the analysis was carried out on the overall time series before being averaged, we do not present the cones of influence here, and all periodicities in the 1–120-day range can be interpreted as being meaningful.

PC#1 and 2 show large-scale alignments of OLR anomalies (Fig. 1), which are out-of-phase between SA and Madagascar. These patterns are elongated in a north-west to south-east direction and show a clear continuity between the tropical latitudes ( $15^\circ\text{S}$  for instance for PC#1) and the southern mid-latitudes ( $37^\circ\text{S}$ ). Temporally, the associated time series show relatively strong periodicities in the 5–20-day range (Fig. 2). In addition, PC#1 shows a non-negligible intraseasonal signal (30–60-day range). These structures are thus mostly valid at the synoptic timescale, and possibly at the intraseasonal one for PC#1. We thus conclude that, in agreement with previous works (e.g. Washington and Todd 1999; Todd et al. 2004), the first two

**Fig. 1** Loading patterns of a principal component applied on the daily OLR anomaly field. Period of analysis: November through February 1979–1980 to 2006–2007. See text for details. Contour interval is 0.1. *Dashed lines* encompass correlation values that are significant at the 95% level according to a Bravais–Pearson test. The *black boxes* encompass the continental subset for which associated rainfall anomalies are analyzed



PCs represent tropical–temperate interactions, and more precisely, occurrences of synoptic-scale TTT systems.

The fact that two PCs appear associated with TTTs is due to their varying longitudinal location, a key feature as far as consequences for continental rainfall are concerned. For instance, Todd et al. (2004) estimated that a large part of the interannual variability of the rainfall over SA can be directly related to the longitude of these systems. Different possible locations of TTT cloud bands are thus depicted by the pair formed by PC#1 and 2. PC#2 positive scores represent cloud bands located in the west of the domain, over South Africa. PC#1 negative scores depict TTT systems located further east, over Mozambique and the southern Mozambique channel. PC#2 negative scores correspond to cloud bands that reach southern Madagascar and Lake Malawi further north. Lastly, PC#1 positive scores depict cloud alignments over the east of the domain, i.e. near Mauritius. The phase-locking between these two PCs will be examined in Sect. 7 in order to document the life cycle of the TTTs.

PC#3–5 (Fig. 1) represent OLR fluctuations centred on the north-west (PC#3), south (PC#4) and centre (PC#5) of the SA subcontinent. Madagascar and the area to its east experience in-phase (PC#4–5) or out-of-phase (PC#3) signals. Temporally, their associated scores mainly

fluctuate at the intraseasonal timescale (Fig. 2). When compared to PC#1–2, the synoptic variations appear much weaker, and the most energetic frequencies are restricted to the 30–60-day range. Such a timescale is particularly reminiscent of the MJO. The implication of the latter for the five PCs will be discussed in Sect. 5.

#### 4 Atmospheric dynamics and consequences for South African rainfall

Figures 3 and 4, respectively, show the correlation of the five OLR PCs with the horizontal wind at 850 and 300 hPa. Figure 5 presents the correlation with the omega vertical velocity at 500 hPa, used here to monitor deep atmospheric convection in the troposphere. The same analysis applied to the different layers of the troposphere showed very similar results, indicating that the vertical motion anomalies observed in Fig. 5 can be generalised to other levels and, hence, can be interpreted as deep ascending/subsiding motion. For these three figures, we chose to represent the atmospheric patterns on a larger domain, to show in which large-scale configurations the Southern African convective anomalies are embedded. This configuration is of importance, especially in the north of the domain, as atmospheric

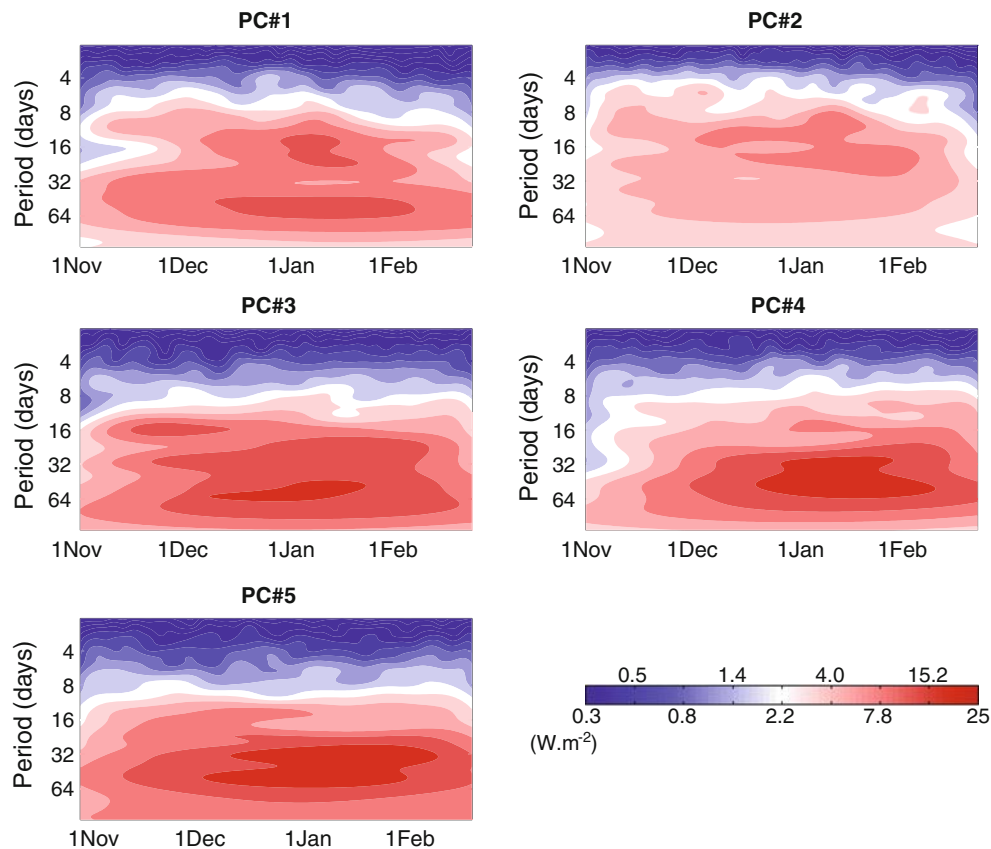


**Fig. 2** Wavelet analysis ( $\text{W m}^{-2}$ , with a logarithmic representation) of the score series associated with the five PCs. All analyses are carried out on normalized data for the NDJF 1979–1980 to

2006–2007 period, and the wavelet scalogram was then averaged over the 28 years. See colour legend for shading

anomalies over tropical Africa can relate to the moisture fluxes reaching the SA region from the tropical latitudes (e.g. Pohl et al. 2007; Vigaud et al. 2007).

Figure 6 displays the rainfall differences over South Africa between the positive and negative phases of each of the five OLR PCs. Unfortunately, only rain-gauge records over South Africa and neighbouring areas are of sufficiently high resolution; thus, Fig. 6 has a smaller domain than the other figures. These in situ observations were nevertheless preferred to satellite estimates, because the latter are strongly dependent on the OLR field and would thus be strongly overlapping the loading patterns shown in Fig. 1. As the domains are of different size, the region for which rainfall anomalies were monitored is shown as boxes in Fig. 1. We first extracted the strong positive ( $>1$ ) and strong negative ( $<-1$ ) scores for the five PCs, and then calculated the difference in the daily rainfall amounts. Composite analyses were preferred to linear correlations, because of the non-Gaussian distribution of the daily rainfall records. Following Wheeler et al. (2008), we tested the significance of the rainfall anomalies using a non-parametric resampling approach that consists of shifting the time series 400 times, and then re-calculating the

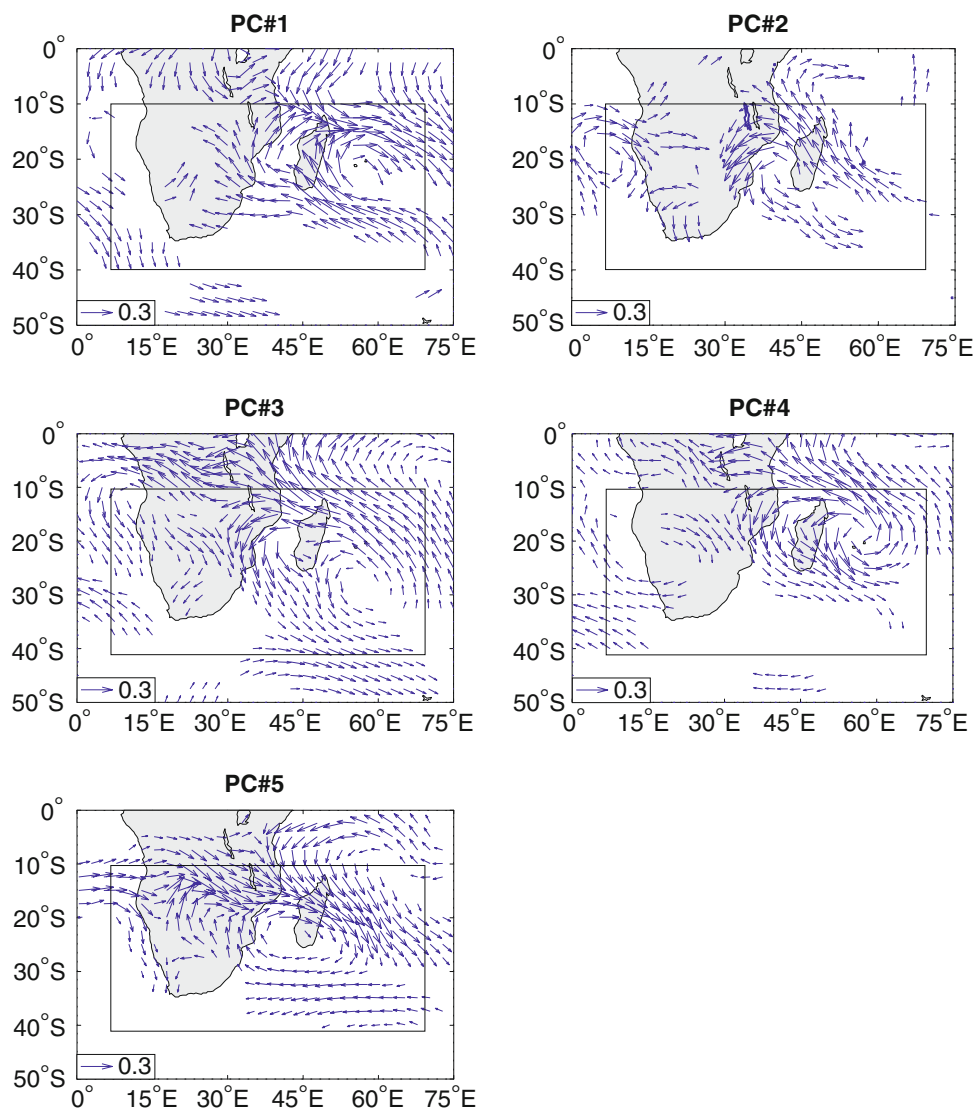
anomaly values. These 400 synthetic realisations are then sorted and the 95th percentile value used as the significance threshold at the 95% confidence level.

The number of days included in this analysis (i.e. the number of days during which the absolute value of the scores is higher than one standard deviation) significantly vary interannually, and is thus shown on Fig. 7. Note that the average values are typically comprised between 20 and 30 days per season. These fluctuations in the extreme score values, from one NDJF season to another, demonstrate that the OLR PCs have a marked interannual component, which will be examined in Sect. 6.

PC#1–2 generally show wind patterns with the same sign in the lower and the higher layers of the troposphere, while the sign is reversed for PC#3–5 (Figs. 3, 4). This statement is confirmed by geopotential height anomalies (not shown), which are in phase throughout the troposphere for PC#1–2 but are out-of-phase between the upper and the lower levels for the three following PCs. Between the equator and  $10^{\circ}\text{S}$ , PC#3–4 are associated with marked anomalies in the vertical component of the wind (Fig. 5), which is not the case with PC#1–2. Hence, we hypothesize that mid-latitude dynamics is implicated in PC#1–2, and



**Fig. 3** Correlation of the five OLR PCs on the horizontal wind field at 850 hPa, NDJF 1979–1980 to 2006–2007. The only correlations that are significant at the 95% level according to a Bravais–Pearson test are shown. The *black boxes* encompass the domain over which the OLR PCs were calculated

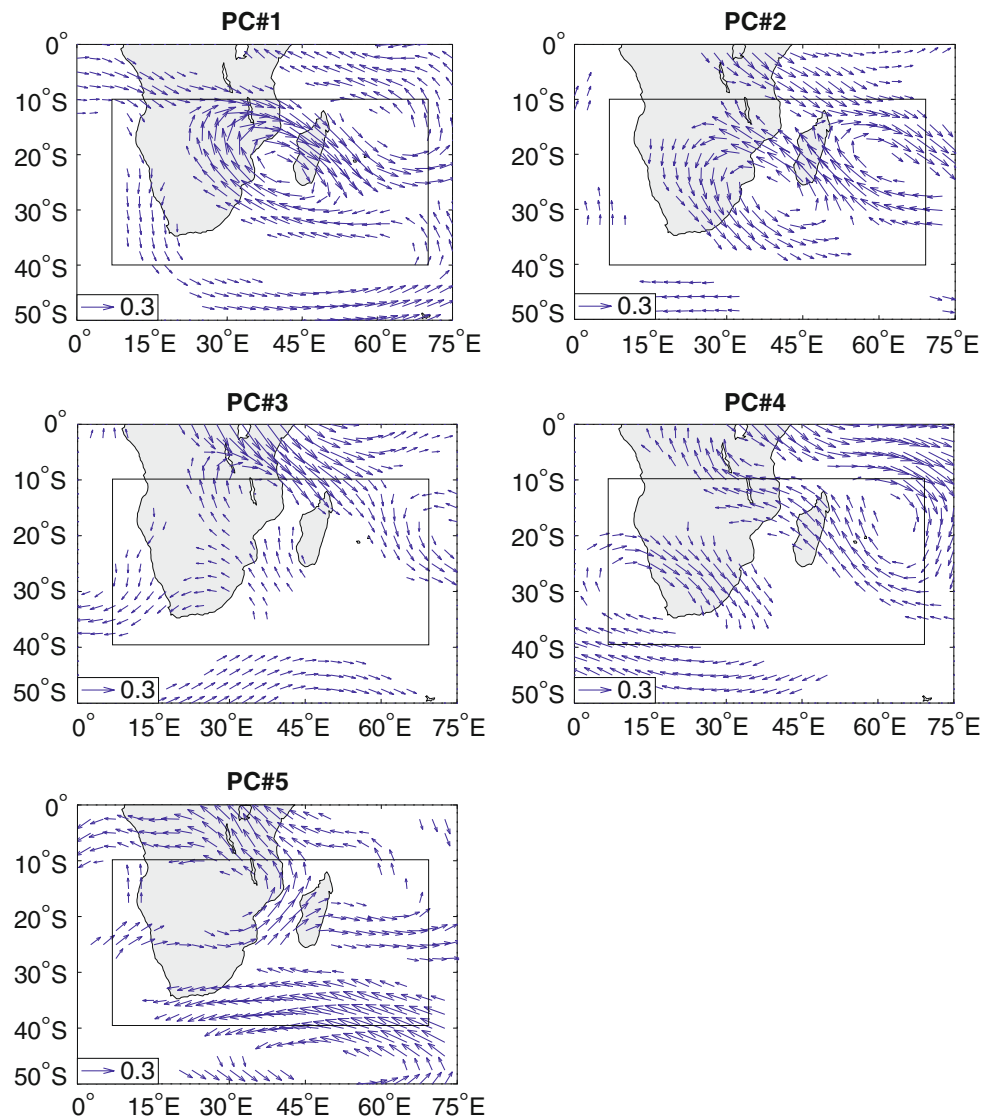


generates in-phase geopotential and pressure fluctuations over the whole depth of the troposphere, while large-scale overturning circulation cells, often observed in the tropics, could be the origin of the reversed sign and upward motion anomalies for PC#3–4, and, to a lesser extent, PC#5. The vertical component of the wind (Fig. 5) is generally consistent with the OLR spatial structures (Fig. 1) for the five PCs, a coherent result as the PCA basically extract convective signals. To verify these hypotheses, we now examine these patterns more in detail, together with the anomalies in vertical motion and rainfall (Fig. 6).

During its positive phase, the enhanced convection associated with PC#1 is embedded in lower-layer cyclonic circulation anomalies over the Mascarene High, resulting in north-westerly anomalies over the tropical Indian Ocean in the east of the domain (Fig. 3). For the negative phase, anticyclonic anomalies occur over the Mascarene High, and north-westerly anomalies are found further west, from

the SA region to the southern Mozambique Channel and the south of Madagascar. In both cases, poleward transport anomalies take place in the lee of the band of enhanced convection, consistent with the results of Todd and Washington (1999) concerning the circulation anomalies associated with the TTT systems. Similar results were also confirmed in Fauchereau et al. (2008): their cluster#5 (depicting west-located TTT systems) corresponds to the negative phase of PC#1, and the lower-layer wind anomalies are quite alike, especially over Madagascar and the SWIO. In addition, we document here the upper-layer dynamics. A very strong anomaly cell (cyclonic for the positive phase, anticyclonic for the negative phase) located over the Mozambique Channel enhances the poleward motion near the center of the enhanced convection region. This statement is true during both phases of the PC. East of the Mascarene High, a reverse cell occurs over the southern Indian Ocean. The structure is thus slightly shifted towards

**Fig. 4** As Fig. 3 but for the wind at 300 hPa



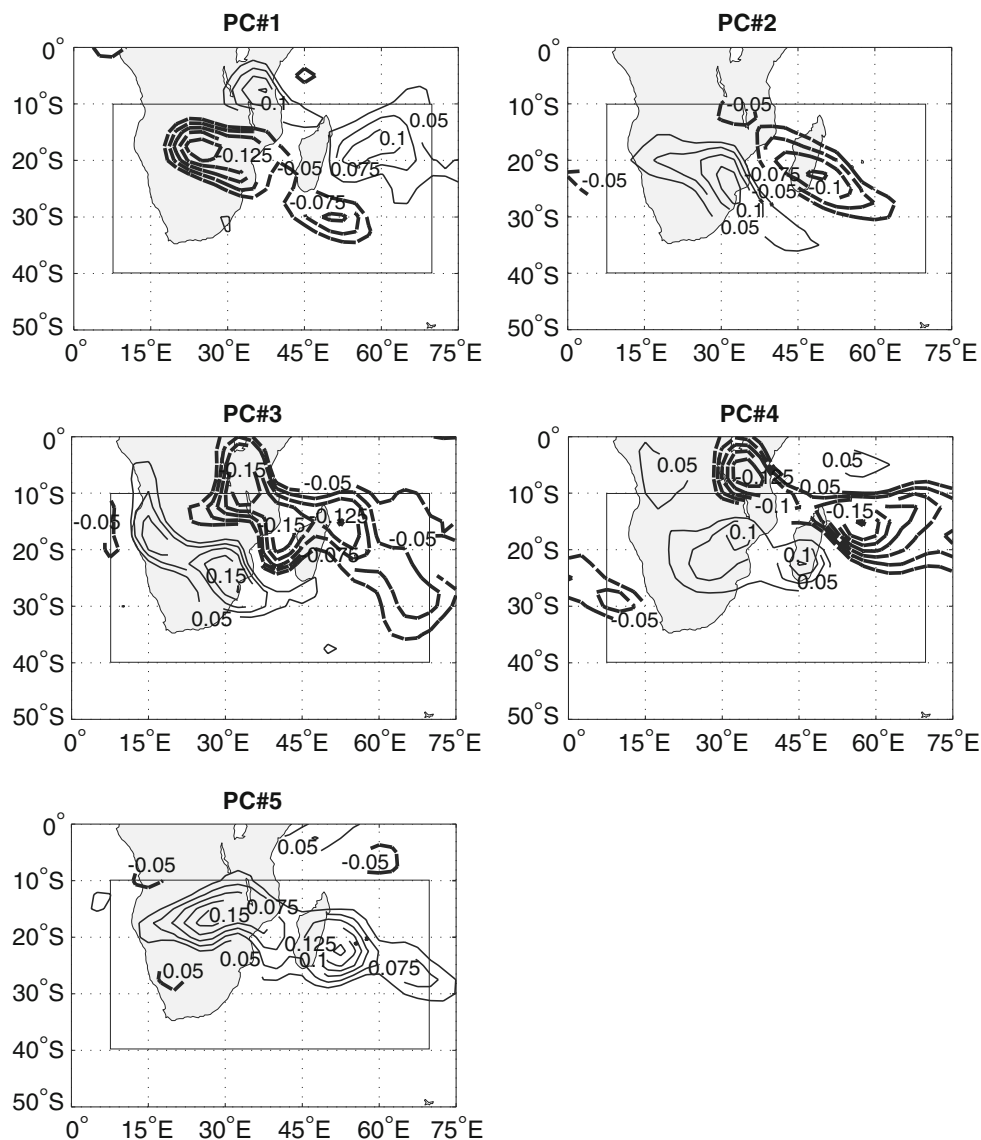
the west compared to the lower-layer atmospheric pattern and is clearly reminiscent of the mid-latitude troughs, confirming that the TTT systems occur concomitantly with a semi-stationary wave in the upper layers (Lyons 1991). The vertical component of the wind shows an out-of-phase dipole quite consistent with the corresponding OLR anomalies shown on Fig. 1, upward motion being located during both positive and negative phases of the PC in the enhanced convection band. The wind patterns are shifted 5° northwards compared to the OLR loadings: the strongest signals are for instance located over Botswana, Zambia and Zimbabwe. Similarly, the rainfall signals also shifted slightly relative to the OLR structure. Over South Africa and neighbouring countries, where high resolution rain-gauge records are available (Fig. 6), most of the area experiences wet (dry) conditions during the positive (negative) phase of PC#1. Dry conditions are restricted to the

north of the country, near the positive OLR loading area shown in Fig. 1.

Given the weakness of the OLR and vertical motion signals over South Africa, one can conclude that the modulation of the daily rain is not directly attributable to deep atmospheric convection. Instead, it is more obviously related to lower-layer moisture convergence (Fig. 3), as confirmed by significant positive moist static energy and specific humidity anomalies associated with this PC in the lower layers (not shown). The reverse situation is found for negative phases: the north of the country experiences wet conditions due to convective activity (Figs. 1, 5) and dry conditions are prevalent over the other parts of South Africa, in association with divergence in the lower levels.

Roughly opposite circulation patterns are found for PC#2, but they are generally shifted towards the west. This symmetry corresponds to a different location and/or a

**Fig. 5** Correlation of the five OLR PCs on the vertical component of the wind at 500 hPa, NDJF 1979–1980 to 2006–2007. Contour interval is 0.05. The only correlations that are significant at the 95% level according to a Bravais–Pearson test are shown. *Dashed lines* (negative correlations) correspond to subsiding anomalies when positive score values are considered. The *black boxes* encompass the domain over which the OLR PCs were calculated



different phase in the life time of the TTT systems. The poleward transport anomalies in the lower-layers are also located east of the enhanced convection area, and the wave structure in the upper-layers is here more obvious. It was already described in Fauchereau et al. (2008), as the negative phase of PC#2 is very close to their cluster#7 (describing the occurrences of east-located TTT). The vertical wind anomalies are in better agreement with the OLR spatial configurations, though they are located further north. South Africa and neighbouring countries experience in-phase rainfall anomalies (Fig. 6), the most pronounced being confined to the north where both air specific humidity and rainfall seasonal amounts are the highest.

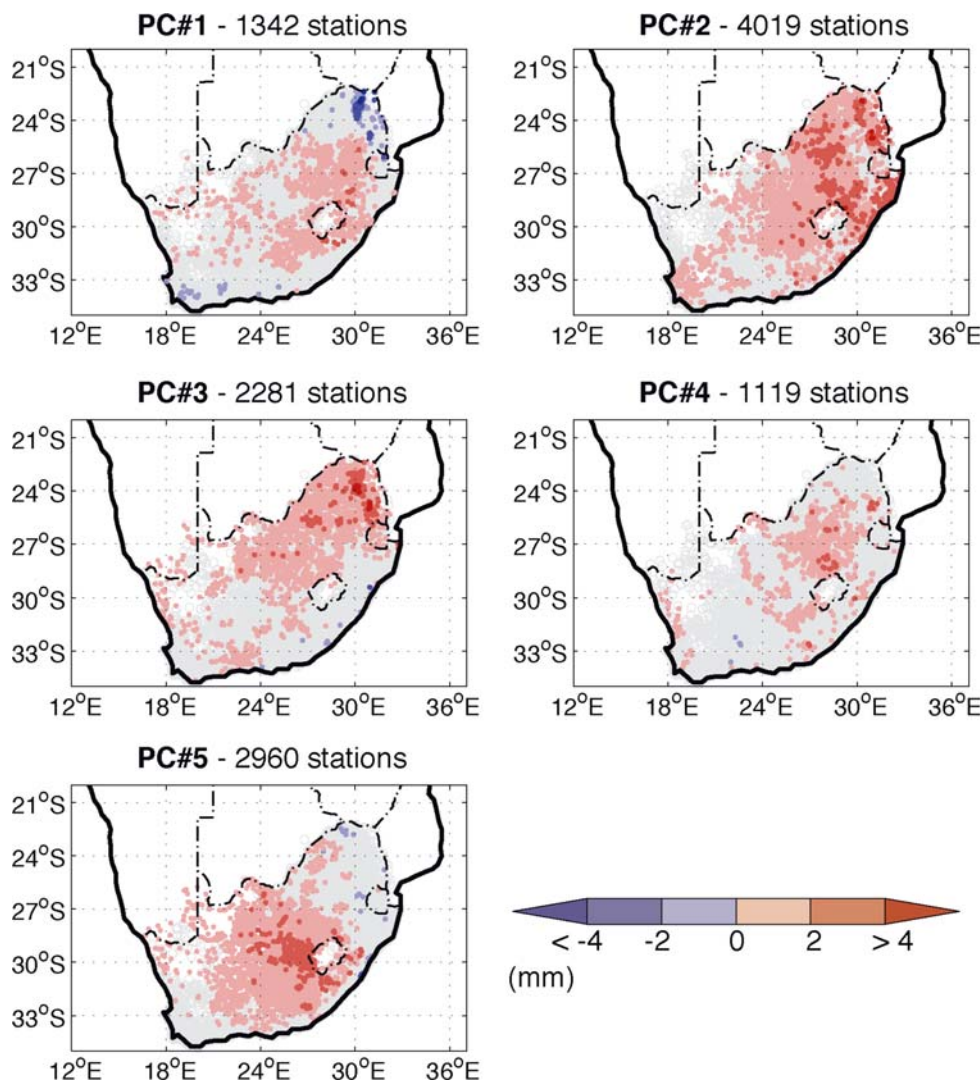
The correspondence between the OLR structures and the rainfall and vertical velocity anomalies remains imperfect. Besides, the horizontal wind fields show correlation values

that remain weaker (though highly significant) than those calculated with the horizontal component of the wind for both PC#1 and 2. These results suggest that the rain-causing mechanisms are not purely convective, and moisture transport in the lower-layers of the tropical troposphere is as fundamental as vertical air motion to explain the rainfall anomalies associated with the TTT systems. As for PC#1, lower-layer northerly fluxes located over tropical Africa (and especially the Great Lakes region) are seen to favour wet conditions over subtropical SA, by conveying moisture from the lower latitudes towards the tropics. Southerly fluxes are on the contrary associated with dryness.

The circulation anomalies of PC#3 and 4 show strong similarities. Their positive phases (inducing positive rainfall anomalies over South Africa, Fig. 6) are associated



**Fig. 6** Difference of daily rainfall amount (mm) over the SA region between the positive (>1) and negative (<-1) score values for the five OLR PCs, period NDJF 1979–1980 to 1998–1999. Only significant anomalies are here shown, according to a non-parametric resampling approach at the 95% level. The number of stations (out of 7,665) significantly associated with each of the PCs is indicated on the figure. See text for details and colour legend for shading

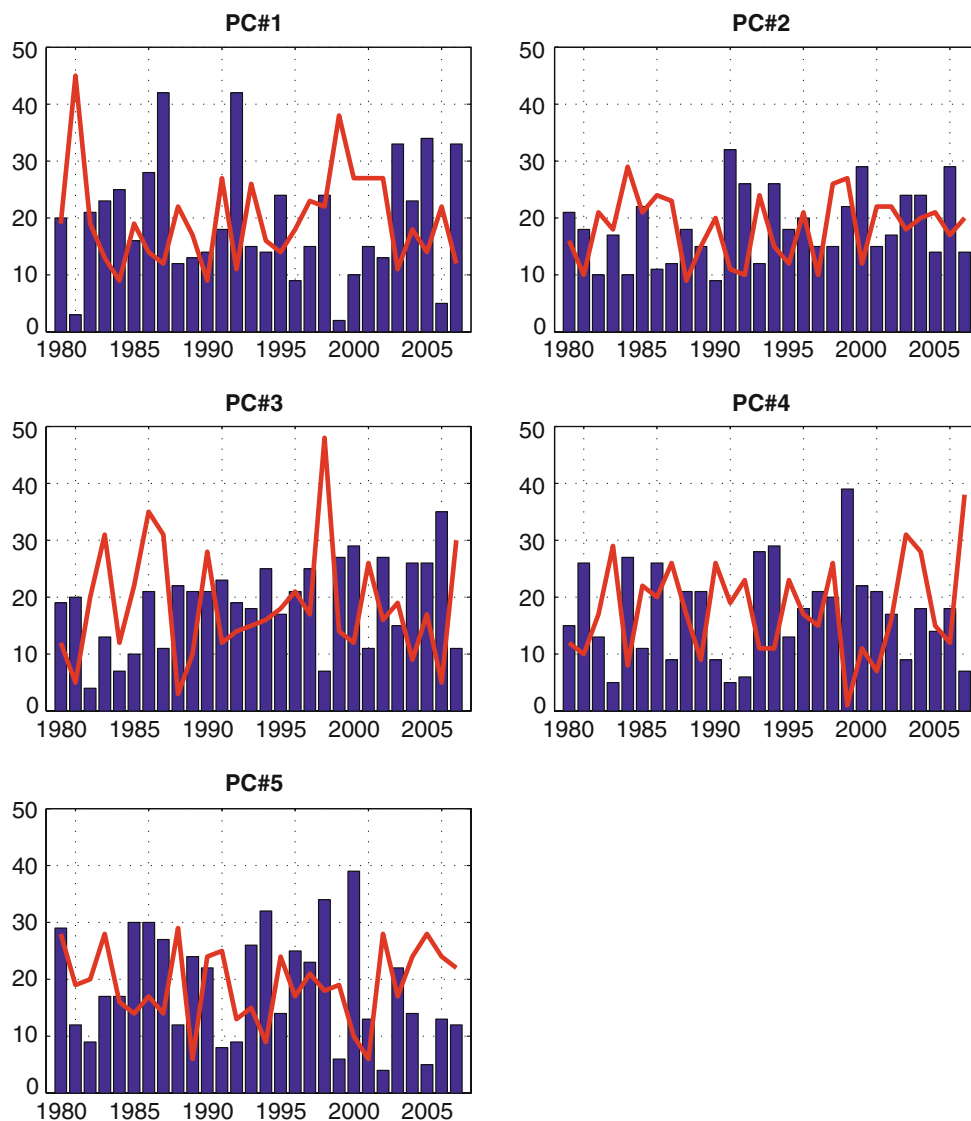


with lower- (upper-) layer easterly (westerly) anomalies over the tropical Indian Ocean, suggesting large-scale cell circulations. Over tropical Africa, the sign between the low and the higher levels of the troposphere is also reversed, and northerly (southerly) anomalies are found at 850 (300) hPa. Such patterns were already discussed in Pohl et al. (2007) and were attributed to an intraseasonal modulation of the Mascarene High by the MJO, a hypothesis fully consistent with the cellular nature of the circulation anomalies in the tropics. In addition, geopotential height anomalies display clear and coherent signals over the SWIO, with maximum amplitudes located over the Mascarene High region (not shown). Lower-layer convergence, as well as marked vertical motion signals, also contributes to the wet conditions generated by these patterns. Section 5 will examine the implication of the MJO to validate these hypotheses. Note that the amplitude of the correlations with the vertical component of the wind is higher than for

PC#1–2, suggesting a stronger influence of atmospheric convection in these two PCs.

Finally, PC#5 shows a rather different pattern. Rainfall modulation is through deep convection over tropical Africa (Figs. 1, 5) but remains significant as far south as South Africa (Fig. 6), where OLR anomalies are still rather strong in spite of weak vertical velocity signals. Based on Figs. 3 and 4, and moist static energy content in the lower layers of the troposphere (not shown), unstable conditions result from moisture transport from the tropical South East Atlantic, and associated northerly fluxes along the Angolan/Namibian coast. Moisture convergence also occurs in the low levels (Fig. 3) and divergence in the high troposphere (Fig. 4). The convective fluctuations over northern Madagascar and to its east are favoured by very strong convergence in the lower troposphere and marked upward motion in the mid-layers. The reverse situation is found during the negative phase of the PC.

**Fig. 7** Bars number of days with score values higher than one standard deviation for the five PCs for each NDJF season on the period 1979–1980 to 2006–2007. Line as bars but for values below minus one standard deviation



## 5 Relationship with the MJO

The MJO signal over the region was first suggested in Levey and Jury (1996) who identified significant periodicities in the 30–60-day range in the rainfall and evaporation fields over the SA region and confirmed more recently by Pohl et al. (2007). The influence of the MJO on SA rainfall intraseasonal variability occurs through a modulation of the lower-layer moisture fluxes from the low latitudes (see Sect. 1). The relationship between the large-scale forcing induced by the MJO and the more regional synoptic-scale TTT systems remains, however, to be analysed. The part of the OLR variability attributed to the MJO also needs to be quantified. These two aspects are the scope of the present section.

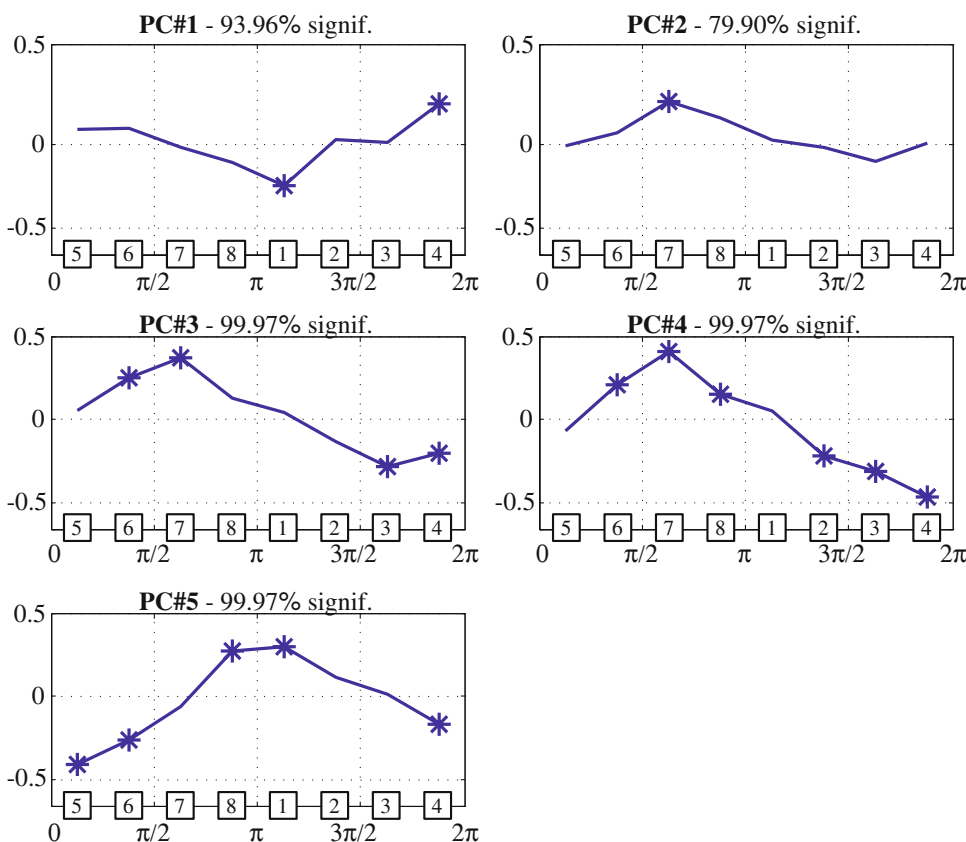
Figure 8 shows the results of a composite analysis of the time series of each PC for the different MJO phases according to the *RMM* indices described in WH04. Over

the SA region, the peak of rainfall associated with the MJO is found at phase  $\pi$  and the dry conditions at phase  $2\pi$  (Pohl 2007).

The first two OLR PCs show very weak association with the MJO, the eight phases of WH04 failing to discriminate the score values at the 95% level according to an analysis of variance (ANOVA) (Fig. 8). The occurrences of TTT systems, identified as the days for which the score values are higher (lower) than one (minus one) standard deviation (e.g. Todd and Washington 1999), are also homogeneously distributed over the phases of the MJO and do not concentrate during given phases of the intraseasonal oscillation (not shown). These results suggest that the TTT systems are statistically independent of the MJO, i.e. their occurrences are as likely to occur during any phase of the MJO.

In contrast, PC#3, 4 and 5 show significant associations with the MJO. For these three PCs, low OLR values (i.e.

**Fig. 8** Composite analysis of the scores of the five OLR PCs against the eight MJO phases defined in WH04. Asterisks denote score values that are significantly different from the mean (0) at the 95% level according to a *t* test. The upper labels correspond to the MJO phases as defined by WH04, while the lower labels give the MJO phase in polar notation from 0 to  $2\pi$  radians. The estimated confidence level of the discrimination of the score values by the eight MJO phases according to an ANOVA is labelled on the figure



positive scores for the three PCs) are concentrated in the  $\pi/2$  to  $\pi$  phase bin, i.e. before and during the enhanced convective phase of the MJO over the region. On the other hand, high OLR values are mainly recorded during phases  $3\pi/2$  to  $\pi/2$ , depending on the PC considered, i.e. during the suppressed convection phase of the MJO.

These three PCs are not perfectly in phase over the MJO cycle. The convective phase occurs for example from  $\pi/4$  to  $3\pi/2$  for PC#3 (phases 6–7 according WH04’s notation),  $\pi/4$  to  $\pi$  for PC#4 (phases 6–8), and  $3\pi/4$  to  $5\pi/2$  for PC#5 (phases 8–1). At the intraseasonal timescale, the three configurations seem therefore to succeed each other within the MJO life cycle. The same is also true for the suppressed convection phase over SA. The respective spatial patterns of these PCs (Fig. 1) reveal that this temporal succession describes first a convective cluster located over the southern Angola–northern Namibia region (PC#3), and then a southward propagation towards South Africa (PC#4), and finally a tendency to propagate towards the north (PC#5). These results are fully consistent with the mean propagative characteristics of the MJO-associated convective clusters over the area, such as depicted in Pohl et al. (2007). The wind patterns associated with PC#3 and 4 in the lower layers (Sect. 4) is also consistent with those shown in Pohl et al. 2007 to be favoured by the MJO during

its phase of enhanced convection over SA. In that respect, PC#5 appears as a noticeable exception, and its association with the MJO seems less clear.

From the analysis of Fig. 8, it is thus concluded (1) that the TTT systems and the MJO seem to be independent modes of climate variability over SA, as PC#1–2 show no clear phase-locking with MJO activity; (2) that PC#3 and 4 are significantly associated with the MJO; (3) that the implication of the MJO in PC#5, though statistically significant, needs to be viewed with caution. In order to confirm these results, and quantify the part of variance that is common with the MJO, cross-spectrum analyses are computed between the *RMM1* MJO index and the score time series of the five PCs. The results are displayed in Fig. 9.

At the intraseasonal periodicities of the MJO, PC#1 and 2 present a very low common variance with the *RMM1* index (less than 10%). These results are not statistically significant at the 95% level according to the Monte-Carlo random simulations. The phase relationship with *RMM1* is not constant over the 30–60-day range, pointing to the absence of clear phase-locking. Statistically, the first two PCs are thus independent of the global-scale MJO activity, confirming that the TTT systems are equally likely to occur during all the phases of the MJO.

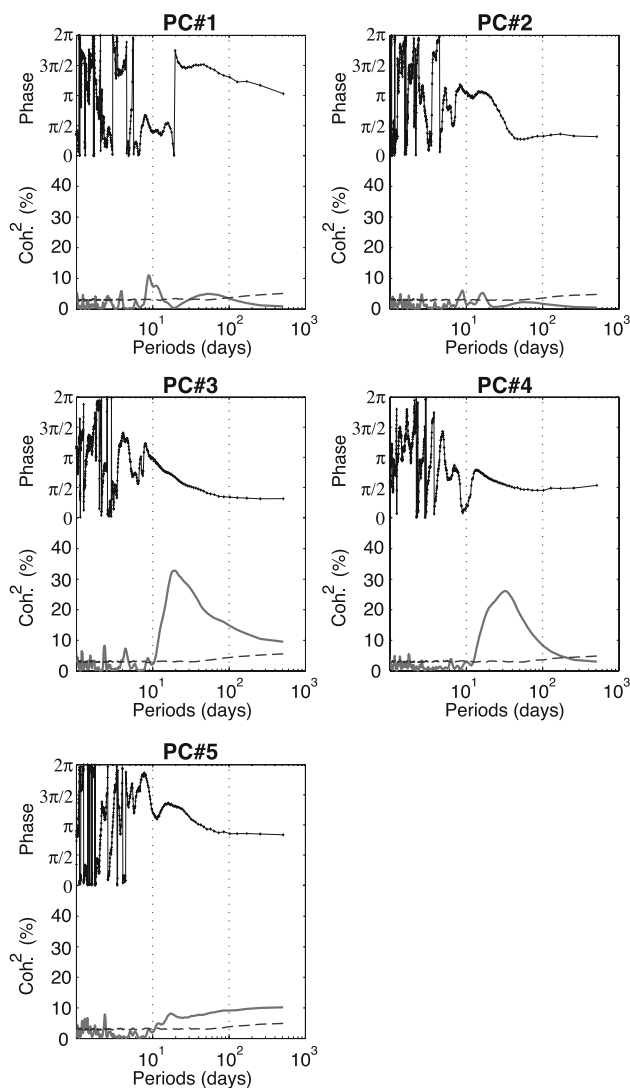


**Fig. 9** Cross-spectrum analysis of the scores of the five OLR PCs and the MJO index *RMM1* defined in WH04. All analyses are carried out on normalized data for the NDJF 1979–1980 to 2006–2007 period, with other months padded with zeros. *Grey lines* square coherence. *Dashed lines* indicate the 95% level according to 1,000 random time series obtained as permutations of the original time series, and having the same lag-1 serial correlation. *Solid black line* with plus signs: phase relationship in radians

PC#3 and 4 show a rather strong and significant association with *RMM1*. At intraseasonal frequencies, their time series share between 30 and 40% of their variance with the MJO index, a result highly significant according to the Monte-Carlo simulations. The phase relationship is almost constant, with an average value of  $\pi/2$ . This result shows that the peak of convection over SA occurs one quarter of cycle after the maximum score value of *RMM1*, i.e. during the MJO phase that is indeed associated with enhanced convection over Africa (see WH04, their Fig. 8).

As already stated above, PC#5 shows a less clear relationship with the MJO, the common variance between the

two time series peaking at only 10%. The phase relationship slightly fluctuates even in the only intraseasonal range, with values mostly comprised between  $\pi/2$  and 0. The association of this configuration with the large-scale MJO is thus weak.

## 6 Relationship with El Niño southern oscillation

Are the synoptic (PC#1–2) and intraseasonal (PC#3–5) variability of Southern African convection modified by the interannual variability (e.g. the background climate conditions, the state of ENSO, ...)? Figure 7 suggested that the five OLR PCs have a marked interannual component. To examine this question, the daily values of the scores were first averaged for each 4-month season, providing inter-annual time series.

To assess the relationship of ENSO with the low-frequency component of the daily PCs, Fig. 10 shows the seasonal mean score values together with the seasonal mean MEI. Though the MEI is usually used because it better documents the coupled nature of ENSO, it is noted that very similar results are obtained with other ENSO indices such as the SST in the Niño3.4 region (not shown). The interannual correlations between the six time series shown in Fig. 10 (i.e. MEI and the 5 OLR PCs) are displayed in Table 1. The teleconnections between the seasonal mean scores and the seasonal mean SST field are displayed in Fig. 11. Partial teleconnections in presence of the MEI (i.e. partial linear correlations, calculated independently of the variance of the MEI) are shown in Fig. 12, in order to remove the specific role of ENSO in the correlations.

Tables 2 and 3 also present the composite mean score values for separate El Niño and La Niña years, as well as the number of days during which the score reaches strong positive ( $>1$ ) and negative ( $<-1$ ) values. Interestingly, the seasonal mean score and the number of days during which the score values are above one or below minus one provide different estimates of the interannual components of the PCs. This is especially true for PC#3 and 5, for which the seasonal mean scores are modified during El Niño and La Niña years, but the frequency of their opposite phases is unchanged (see Tables 2, 3). For PC#1 and 4, however, these different metrics lead to similar results (both mean scores and frequencies being modulated by ENSO). These results suggest that PC#3 and 5 depict interannual fluctuations in the seasonal mean atmospheric convection, while PC#1 and 4 show that the number of synoptic-scale (PC#1) or intraseasonal (PC#4) convective events is directly modulated by the seasonal background conditions and ENSO. In other words, the interannual component of PC#1 and 4 primarily relate to modifications in the frequency of

**Fig. 10** Time series of the seasonal average of the scores (bars) and the MEI (solid line) for the period NDJF 1979–1980 to 2006–2007

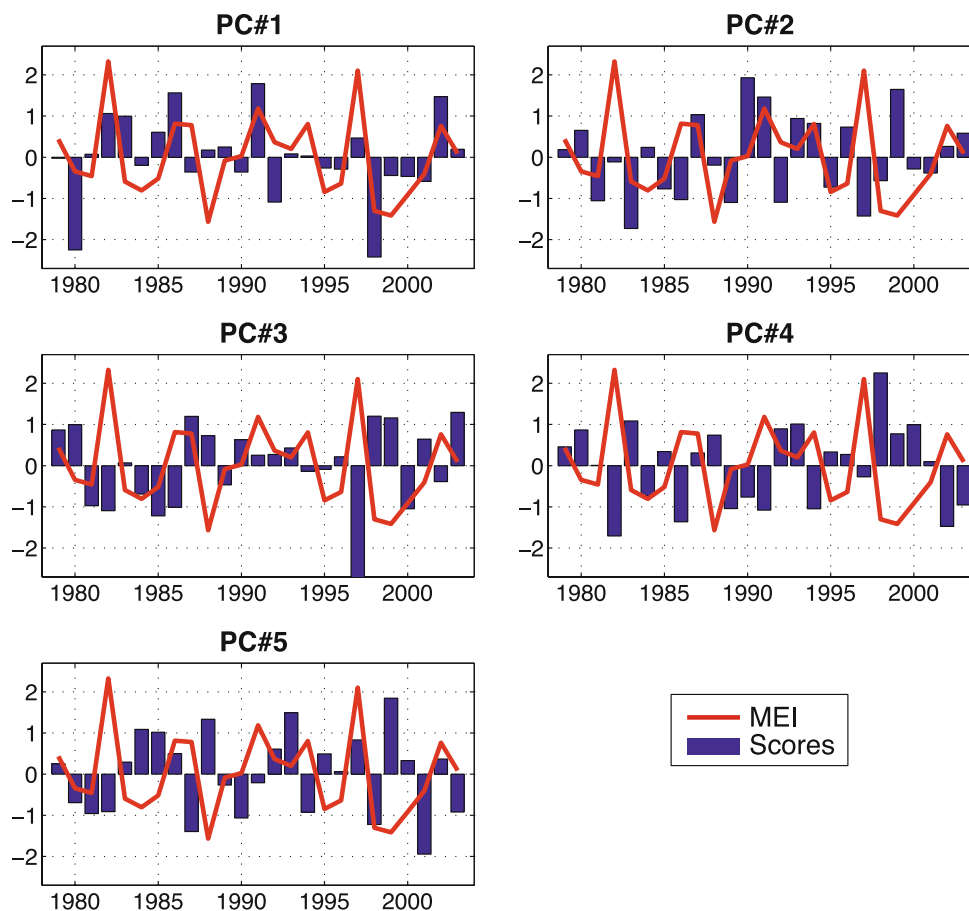


**Table 1** Correlations between the MEI and the seasonal mean score of the five OLR PCs, period NDJF 1979–1980 to 2006–2007

	MEI	PC#1	PC#2	PC#3	PC#4	PC#5
MEI	1.00	<b>0.496</b>	0.005	<b>-0.426</b>	<b>-0.629</b>	-0.216
PC#1		1.00	-0.091	<b>-0.462</b>	<b>-0.678</b>	0.244
PC#2			1.00	<b>0.544</b>	-0.150	-0.090
PC#3				1.00	0.370	-0.252
PC#4					1.00	0.178
PC#5						1.00

Correlation values significant at the 95% level according to a Bravais–Pearson test are in bold

short-lived convective events, while PC#3 and 5 more directly relate to fluctuations in the seasonal mean convection. PC#2 seasonal score and opposite phases are not statistically modified between El Niño and La Niña years.

The successive PCs are now analysed. PC#2 shows no clear teleconnections with the global-scale SST field (Figs. 11, 12), which can also be verified with the other metrics used to quantify its interannual component (i.e. the number of days spent in the opposite phases of these configurations, not shown). It is thus concluded that the low-frequency fluctuations described by PC#2 (Fig. 10)

do not relate to the large scale background conditions but more to the regional mid-latitude dynamics. PC#5 only shows a signal in the tropical North Atlantic (Fig. 11) between 10°N and 30°N. When the influence of ENSO is removed (Fig. 12), these teleconnections remain unchanged, demonstrating their lack of association with El Niño events; an additional signal appears in the western side of the three ocean basins at the southern subtropical latitudes, corresponding to in-phase fluctuations in the three ocean basins. A roughly similar pattern was described in Fauchereau et al. (2003) and was seen to be attributed to a northward shift and a weakening of the subtropical highs. This result is fully compatible with the atmospheric patterns associated with PC#5 and shown in Figs. 3 and 4.

On the other hand, PC#1, 3 and 4 show clear associations with ENSO (Table 1, Figs. 11, 12). The positive (negative) phase of these configurations are favoured during El Niño (La Niña) years for PC#1, and La Niña (El Niño) years for PC#3 and 4. Given the associated rainfall anomalies (Fig. 6), one can conclude that the correlation patterns for PC#3–4 denote the occurrences of seasonal droughts over SA during El Niño years, a result well-known for years (e.g. Dyer 1979; Lindsay



**Fig. 11** Teleconnection patterns between the seasonal mean score of the five OLR PCs (Fig. 10) and the seasonal mean SST, period NDJF 1979–1980 to 2006–2007. *Solid (dashed) lines* encompass positive (negative) correlation values that are significant at the 95% level according to a Bravais–Pearson test

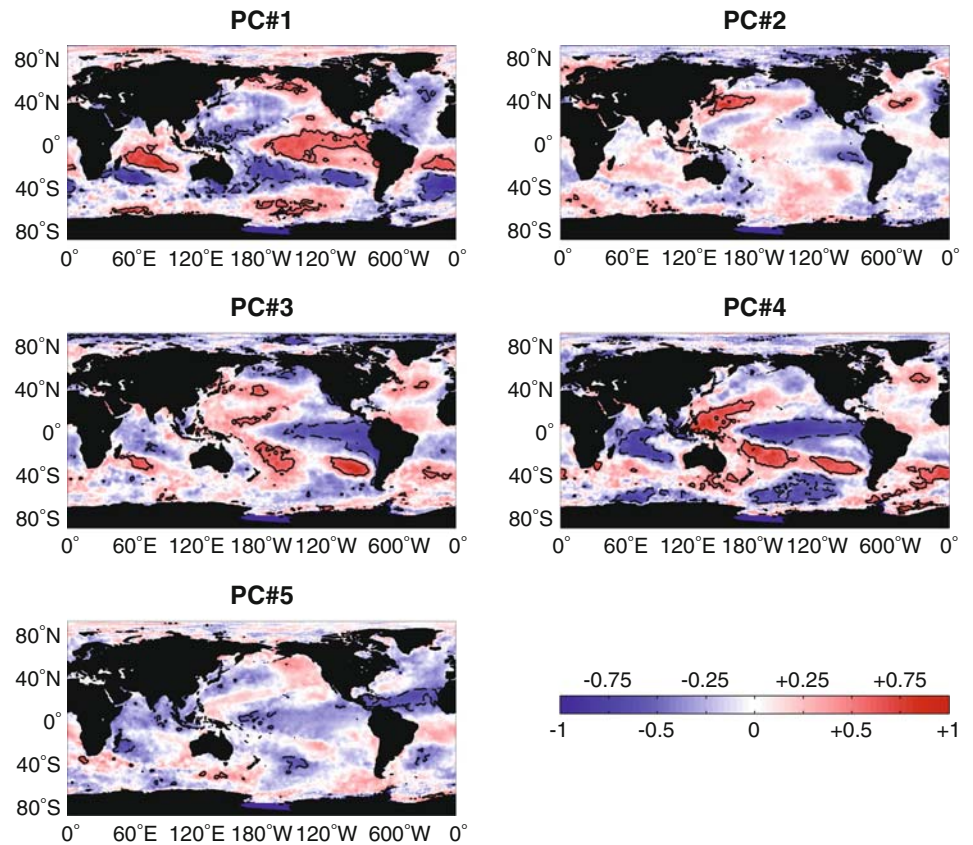


**Fig. 12** As for Fig. 11, but for partial linear correlations in presence of the seasonal mean MEI

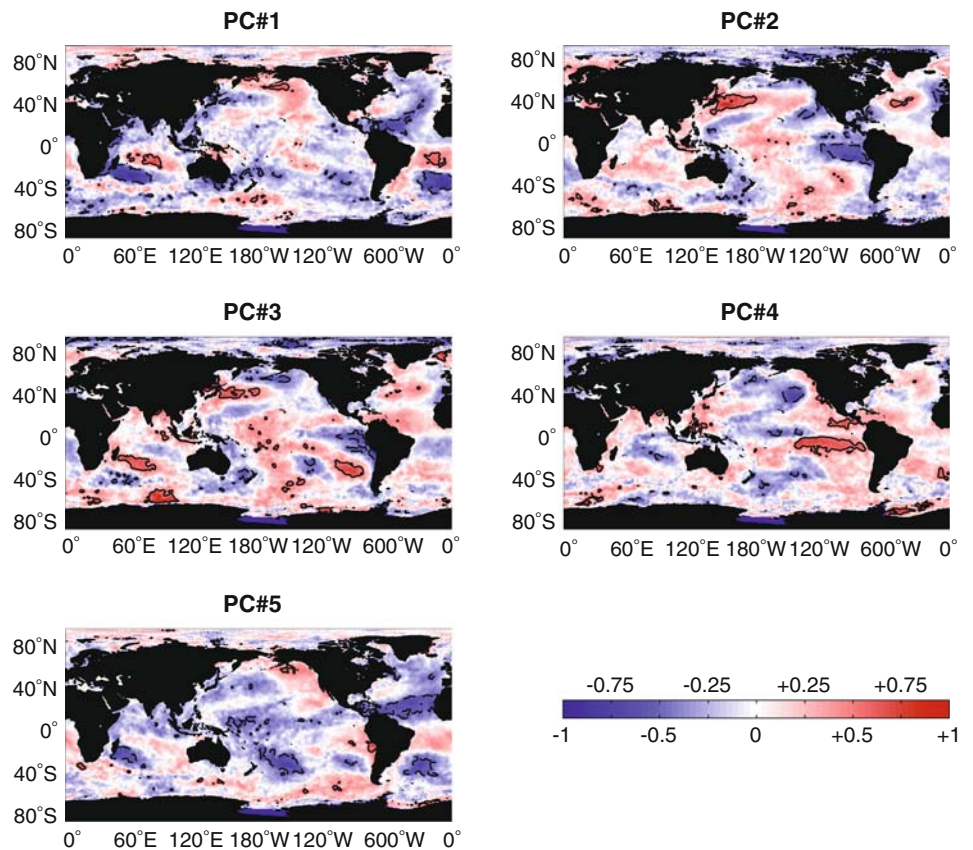


**Table 2** Composite of the score mean values for the five OLR PCs during El Niño (75th percentile of the seasonal mean MEI) and La Niña (25th percentile of the seasonal mean MEI) years, period NDJF 1979–1980 to 2006–2007

	PC#1	PC#2	PC#3	PC#4	PC#5
La Niña	<b>-0.198</b>	-0.001	<b>0.086</b>	<b>0.297</b>	<b>-0.148</b>
El Niño	<b>0.251</b>	-0.007	<b>-0.256</b>	<b>-0.283</b>	<b>-0.009</b>

Significant differences at the 95% level according to a *t* test are in bold

**Table 3** Frequency of the days during which the score values are superior to 1 or inferior to -1 (as shown on Fig. 7) during El Niño and La Niña years

(%)	PC#1	PC#2	PC#3	PC#4	PC#5
Score >1					
La Niña	<b>9.8</b>	20.2	21.8	<b>24.2</b>	21.4
El Niño	<b>31.0</b>	17.6	13.4	<b>10.6</b>	20.2
Score <-1					
La Niña	<b>25.4</b>	19.4	16.6	<b>9.0</b>	11.6
El Niño	<b>14.4</b>	17.8	28.4	<b>25.4</b>	19.4

Samples are defined as in Table 2. Significant differences at the 95% level according to a *t* test are in bold

1988; Lindesay and Vogel 1990). In addition, the opposite phases of PC#4 also describe short-lived wet (dry) spells during La Niña (El Niño) years (Table 3), contributing to the above (below) average seasonal rainfall amounts.

Surprisingly, however, the teleconnections obtained for PC#1 suggest the exact reverse situation, i.e. above-(below-) normal rainfall during El Niño (La Niña) events over South Africa (Fig. 6). Given the spatial loading pattern of the latter configuration (Fig. 1), this paradoxical result is, however, confined in the subtropical part of the domain. During El Niño years, dry conditions are favoured over northern South Africa, Zimbabwe and Mozambique. Wet conditions are favoured over central and southern South Africa and Namibia. PC#3–4 and PC#1 add (cancel) their effects over the north (south) of the domain, a result demonstrating the absence of linearity of the effects of ENSO on the rainfall field over South Africa and contributing to explain the relative weakness of the teleconnection (Mulenga et al. 2003).

## 7 Scale interactions

In this section, we analyse all the temporal interactions between the five PCs for all timescales from daily to

interannual. As the PCs are orthogonal, they are uncorrelated at lag 0; when lags are considered, their score series are, however, likely to show different kinds of associations (e.g. in-phase or out-of-phase variability, quadrature,...) at distinct timescales. In order to document these associations, Fig. 13 presents cross-spectrum analyses computed between the score time series of the five PCs.

At the *synoptic timescale*, the most obvious association between any pair of time series is found for PC#1 and 2, for periodicities comprised between 1 and 2 weeks. More specifically, for periods comprised between 5 and 8 days, the two series show up to 70% of common variance. Their phase relationship is remarkably stable at  $\pi/2$  radians. A maximum score value for PC#2 occurs then a few days after a maximum score value on PC#1. Given their respective loading patterns (Fig. 1), this result must be interpreted as a tendency for TTT systems to propagate towards the east, from the SA region to the Mozambique Channel and Madagascar. These propagative properties have been already discussed in Fauchereau et al. (2008).

At *intraseasonal timescales*, PC#3 shows significant associations with PC#4 and 5. These three time series were all shown to be significantly associated to some extent with the global-scale MJO activity (Figs. 8, 9), which helps to explain why they tend to fluctuate at similar timescales. It is, however, to be noted that their common variance only reaches 15–30%, which confirms that the MJO is not the only forcing mechanism that determines the temporal behaviour of these configurations. This may be particularly true for PC#5, for which the association with the MJO is questionable (Fig. 9). PC#3 is also associated with PC#1 at frequencies centred on 20 days, an ambiguous timescale as it is slightly too long to correspond to the quasi-biweekly oscillation (e.g. Chatterjee and Goswami 2004), and too short to correspond to the MJO. The SA region has also never been identified as an area where the quasi-biweekly oscillation is strong. Because of these uncertainties, we do not discuss this relationship here.

At *interannual timescales*, PC#1 shows significant associations with PC#3 and 4, a result that can be explained by their common relationship with ENSO (see, e.g. Fig. 11). PC#1 (3–4) time series are negatively (positively) correlated with the SST field in the Eastern Pacific (Fig. 11). As a consequence, PC#1 and PC#3–4 show out-of-phase relationships at the interannual timescale ( $\pi$  radians on Fig. 13). Though also significant, the associations between these different time series at the higher frequencies (synoptic timescale) remain subject to caution, because of the inconstancy of their phase relationship. A more unexpected association is found between

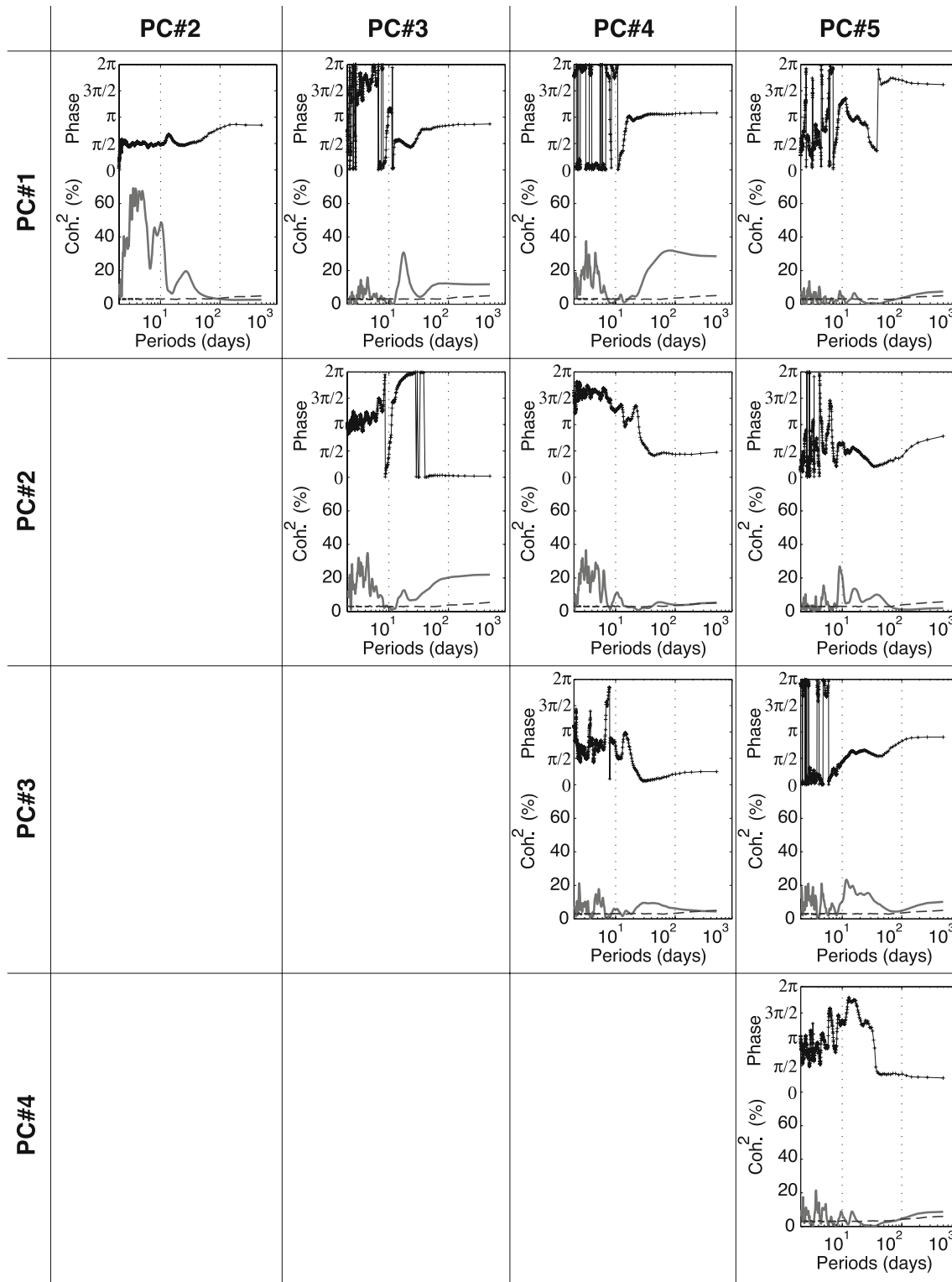


**Fig. 13** Cross-spectrum analyses between the score time series of the five OLR PCs. Analyses computed and significance tested and represented as for Fig. 9

PC#2 and 3 at the interannual timescale. The phase relationship (0) indicates that these two PCs show in-phase fluctuations from 1 year to another. This result,

though difficult to explain, is consistent with their in-phase teleconnections with the Pacific and Atlantic SST field (Fig. 11).

## 8 Summary and discussion

A PCA applied on the daily OLR fields after removal of the annual cycle led to the identification of convective signals at the synoptic, intraseasonal and interannual timescales. Phenomena responsible for these regional convective fluctuations over SA are, respectively, TTT (described by PC#1–2), the MJO (PC#3–4, and more ambiguously, PC#5) and ENSO (depicted by the interannual components of PC#1–3–4). Cross-spectrum analyses were then applied on the score time series associated with these five configurations in order to estimate to what extent these different timescales interact and are embedded in one another.

At the subseasonal (synoptic and intraseasonal) timescales, PC#1 and 2 show a very strong relationship, confined in the synoptic range, and interpreted as a clear tendency for most TTT systems to propagate eastwards. This result is consistent with a recent paper based on a cluster analysis of the large-scale OLR structures over the same region (Fauchereau et al. 2008). Together PC#1–2 show very weak associations with PC#3–4, suggesting that the occurrence of TTT systems is not modulated by the phase of the MJO. This result implies (1) that synoptic-scale TTT systems are as liable to occur during any phase of the MJO; (2) that these two phenomena explain a complementary part of the subseasonal atmospheric and rainfall variability over SA. This may be of primary importance for the implementation of medium-scale forecasting models.

At the interannual timescale, El Niño years are known to favour severe seasonal droughts over SA and many La Niña years correspond to wet summers over the region. However, as discussed in Fauchereau et al. (2008) and confirmed in this study, the response of the rain to the state of El Niño is complex and not purely linear. During El Niño years, PC#3–4 present abnormally low seasonal scores, inducing seasonal dry conditions over SA. The reversed sign is found for PC#1. During El Niño years, dry (wet) conditions are favoured over tropical (subtropical) SA; the reverse situation is found during La Niña years. Consequently, in-phase (out-of-phase) signals are found over the northern (southern) part of the domain, where PC#1 and PC#3–4 add (withdraw) their effects. As a result, the linear relationship between atmospheric convection and ENSO is larger in the tropical part of SA, as confirmed by Fig. 14. Similar conclusions are obtained with satellite-based rainfall estimates (not shown).

Table 3 details how PC#1 weakens the influence of ENSO over subtropical SA. During El Niño years, an abnormally high number of short-lived wet events (as extracted by the days during which the score values are

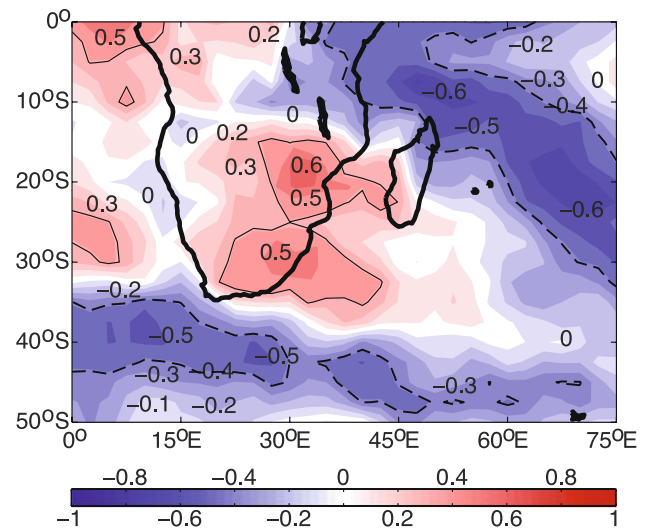


**Fig. 14** Linear correlations between the seasonal mean MEI and the seasonal OLR field. Period of analysis: November through February 1979–1980 to 2006–2007. Contour interval is 0.1. Solid (dashed) lines encompass positive (negative) correlation values that are significant at the 95% level according to a Bravais–Pearson test

higher than one standard deviation) are recorded and favour wet conditions in the south and in the west of SA. These positive rainfall anomalies were attributed in Sect. 4 to lower-layer moisture convergence and do not result in purely convective processes. These wet spells usually last 3–6 days (not shown) and are thus restricted to the synoptic range. These high-frequency fluctuations interfere with the seasonal dry conditions and weaken the regional influence of ENSO. Though the average atmospheric convection is weaker during El Niño years, subseasonal fluctuations in the OLR tend thus to be larger during these years, a result already found in Pohl et al. (2007).

The relationship between ENSO and synoptic-scale activity depicted by PC#1 demonstrates that the latter is (at least partly) modulated by ENSO. It is now questioned to what extent the tropical–temperate interactions are affected: TTT systems could possibly present different properties during El Niño and La Niña years. Additional work needs to be done to provide a more complete description of their preferred location, spatial extent and propagative properties, and to assess the role of ENSO in modulating these characteristics.

**Acknowledgments** This work was carried out at the University of Cape Town as part of the PICS PESOCA exchange programme co-funded by France and South Africa. Benjamin Pohl thanks the staff of the Department of Oceanography at UCT for its hospitality. Nicolas Fauchereau and Mathieu Rouault thank funding from WRC project K5/1747. The authors thank Matt Wheeler (Centre for Australian Weather and Climate Research) and two anonymous reviewers for helpful comments on the manuscript.



## References

- Carvalho LMV, Jones C, Liebmann B (2004) The South Atlantic convergence zone: intensity, form, persistence, and relationships with intraseasonal to interannual activity and extreme rainfall. *J Clim* 17:88–108
- Chatterjee P, Goswami BN (2004) Structure, genesis and scale selection of the tropical quasi-biweekly mode. *Q J R Meteorol Soc* 130:1171–1194
- Cook KH (2000) The South Indian convergence zone and interannual rainfall variability over Southern Africa. *J Clim* 13:3789–3804
- Dyer TGJ (1979) Rainfall along the east coast of Southern Africa, the southern oscillation and the latitude of the subtropical high pressure belt. *Q J R Meteorol Soc* 105:445–451
- Fauchereau N, Trzaska S, Richard Y, Roucou P, Camberlin P (2003) Sea-surface temperature co-variability in the southern Atlantic and Indian Oceans and its connections with the atmospheric circulation in the southern hemisphere. *Int J Climatol* 23:663–677
- Fauchereau N, Pohl B, Reason CJC, Rouault M, Richard Y (2008) Recurrent daily OLR patterns in the Southern Africa/Southwest Indian Ocean region, implications for South African rainfall and teleconnections. *Clim Dyn*. doi:10.1007/s00382-008-0426-2
- Jury MR (2002) Economic impacts of climate variability in South Africa and development of resource prediction models. *J Appl Meteorol* 41:46–55
- Kanamitsu M, Ebisuzaki W, Woollen J, Yang SK, Hnilo JJ, Fiorino M, Potter GL (2002) NCEP-DOE AMIP II reanalysis (R-2). *Bull Am Meteorol Soc* 83:1631–1643
- Levey KM, Jury MR (1996) Composite intraseasonal oscillations of convection over Southern Africa. *J Clim* 9:1910–1920
- Liebmann B, Smith CA (1996) Description of a complete (interpolated) outgoing longwave radiation dataset. *Bull Am Meteorol Soc* 77:1275–1277
- Lindesay JA (1988) South African rainfall, the southern oscillation and a southern hemisphere semi-annual cycle. *J Climatol* 8:17–30
- Lindesay JA, Vogel CH (1990) Historical evidence for southern oscillation-Southern African rainfall relationships. *Int J Climatol* 10:679–689
- Lynch SD (2003) Development of a RASTER database of annual, monthly and daily rainfall for Southern Africa. WRC report N 1156/1/03, 78 pp
- Lyons SW (1991) Origins of convective variability over Equatorial Southern Africa during Austral Summer. *J Clim* 4:23–39
- Madden RA, Julian PR (1994) Observations of the 40–50 day tropical oscillation—a review. *Monthly Weather Rev* 122:814–837
- Mason SJ, Jury MR (1997) Climatic variability and change over southern Africa: a reflection on underlying processes. *Prog Phys Geogr* 21:23–50
- Matthews AJ, Hoskins BJ, Slingo JM, Blackburn M (1996) Development of convection along the SPCZ within a Madden-Julian oscillation. *Q J R Meteorol Soc* 122:669–688
- Matthews AJ (2000) Propagating mechanisms for the Madden-Julian oscillation. *Q J R Meteorol Soc* 126:2637–2652
- Mulenga HM, Rouault M, Reason CJC (2003) Dry summers over NE South Africa and associated circulation anomalies. *Clim Res* 25:29–41
- Pohl B (2007) The Madden-Julian oscillation and regional rainfall variability in Sub-Saharan Africa. PhD thesis, Dept. Geography, University of Burgundy, 283 p
- Pohl B, Richard Y, Fauchereau N (2007) Influence of the Madden-Julian oscillation on Southern African summer rainfall. *J Clim* 20:4227–4242
- Prokoph A, Patterson RT (2004) Application of wavelet and regression analysis in assessing temporal and geographic climate variability: eastern Ontario, Canada as a case study. *Atm Ocean* 42(3):201–212
- Rayner NA, Parker DE, Horton EB, Folland CK, Alexander LV, Rowell DP, Kent EC, Kaplan A (2003) Global analyses of sea surface temperature, sea ice, and night marine air temperature since the late nineteenth century. *J Geophys Res* 108(4407). doi:10.1029/2002DJ002670
- Reason CJC, Allan RJ, Lindesay JA, Ansell TJ (2000) ENSO and climatic signals across the Indian Ocean basin in the global context: part I, Interannual composite patterns. *Int J Climatol* 20:1285–1327
- Reason CJC, Rouault M (2002) ENSO-like decadal patterns and South African rainfall. *Geophys Res Lett* 29(13). doi:10.1029/2002GL014663
- Reason CJC, Jagadheesha D (2005) A model investigation of recent ENSO impacts over southern Africa. *Meteorol Atm Phys* 89:181–205
- Richard Y, Trzaska S, Roucou P, Rouault M (2000) Modification of the Southern African rainfall variability/El Niño southern oscillation relationship. *Clim Dyn* 16:883–895
- Richard Y, Fauchereau N, Pocard I, Rouault M, Trzaska S (2001) XXth century droughts in Southern Africa: spatial and temporal variability, teleconnections with oceanic and atmospheric conditions. *Int J Climatol* 21:873–885
- Rouault M, Richard Y (2003) Spatial extension and intensity of droughts since 1922 in South Africa. *Water SA* 29:489–500
- Rouault M, Richard Y (2005) Spatial extent and intensity of droughts in Southern Africa. *Geophys Res Lett* 32. doi:10.1029/2005GL022436
- Streten NA (1973) Some characteristics of satellite-observed bands of persistent cloudiness over the Southern Hemisphere. *Monthly Weather Rev* 101:486–495
- Todd M, Washington R (1999) Circulation anomalies associated with tropical-temperate troughs in southern Africa and the southwest Indian Ocean. *Clim Dyn* 15:937–951
- Todd MC, Washington R, Palmer PI (2004) Water vapour transport associated with tropical-temperate trough systems over Southern Africa and the southwest Indian Ocean. *Int J Climatol* 24:555–568
- Torrence C, Compo P (1998) A practical guide to wavelet analysis. *Bull Am Meteorol Soc* 79:61–78
- Vigaud N, Richard Y, Rouault M, Fauchereau N (2007) Water vapour transport from the tropical Atlantic and summer rainfall in tropical southern Africa. *Clim Dyn* 28:113–123
- Washington R, Todd M (1999) Tropical-temperate links in southern Africa and southwest Indian Ocean satellite-derived daily rainfall. *Int J Climatol* 19:1601–1616
- Wheeler MC, Hendon HH (2004) An all-season real-time multivariate MJO index: development of an index for monitoring and prediction. *Monthly Weather Rev* 132:1917–1932
- Wheeler MC, Hendon HH, Cleland S, Meinke H, Donald A (2008) Impacts of the Madden-Julian oscillation on Australian rainfall and circulation. *J Clim* (submitted)
- Wolter K, Timlin MS (1993) Monitoring ENSO in COADS with a seasonally adjusted principal component index. In: 17th Climate diagnostics workshop, Norman, OK, pp 52–57
- Zhang C (2005) Madden-Julian oscillation. *Rev Geophys* 43:RG2003. doi:10.1029/2004RG000158